

Second-order topological insulator in twisted bilayer graphene with small twist angle

Fenghua Qi(戚凤华), Jie Cao(曹杰), Xingfei Zhou(周兴飞), and Guojun Jin(金国钧)

Citation: Chin. Phys. B, 2025, 34 (**11**): 116801. DOI: 10.1088/1674-1056/adee03
http://cpb.iphy.ac.cn; http://iopscience.iop.org/cpb

What follows is a list of articles you may be interested in

Molecular beam epitaxial growth and physical properties of AlN/GaN superlattices with an average 50% Al composition

Siqi Li(李思琦), Pengfei Shao(邵鹏飞), Xiao Liang(梁潇), Songlin Chen(陈松林), Zhenhua Li(李振华), Xujun Su(苏旭军), Tao Tao(陶涛), Zili Xie(谢自力), Bin Liu(刘斌), M. Ajmal Khan, Li Wang, T. T. Lin, Hideki Hirayama, Rong Zhang(张荣), and Ke Wang(王科)

Chin. Phys. B, 2024, 33 (**12**): 126801. DOI: 10.1088/1674-1056/ad84cc

Strain compensated type II superlattices grown by molecular beam epitaxy

Chao Ning(宁超), Tian Yu(于天), Rui-Xuan Sun(孙瑞轩), Shu-Man Liu(刘舒曼), Xiao-Ling Ye(叶小玲), Ning Zhuo(卓宁), Li-Jun Wang(王利军), Jun-Qi Liu(刘俊岐), Jin-Chuan Zhang(张锦川), Shen-Qiang Zhai(翟慎强), and Feng-Qi Liu(刘峰奇)

Chin. Phys. B, 2023, 32 (**4**): 046802. DOI: 10.1088/1674-1056/ac7cd4

High repetition granular Co/Pt multilayers with improved perpendicular remanent magnetization for high-density magnetic recording

Zhi Li(李智), Kun Zhang(张昆), Ao Du(杜奥), Hongchao Zhang(张洪超), Weibin Chen(陈伟斌), Ning Xu(徐宁), Runrun Hao(郝润润), Shishen Yan(颜世申), Weisheng Zhao(赵巍胜), and Qunwen Leng(冷群文)

Chin. Phys. B, 2023, 32 (**2**): 026803. DOI: 10.1088/1674-1056/ac9fc1

Extended phase diagram of $La_{1-x}Ca_xMnO_3$ by interfacial engineering

Kexuan Zhang(张可璇), Lili Qu(屈莉莉), Feng Jin(金锋), Guanyin Gao(高关胤), Enda Hua(华恩达), Zixun Zhang(张子璔), Lingfei Wang(王凌飞), and Wenbin Wu(吴文彬)

Chin. Phys. B, 2021, 30 (**12**): 126802. DOI: 10.1088/1674-1056/ac003e

Phase transition-induced superstructures of *β*-Sn films with atomic-scale thickness

Le Lei(雷乐), Feiyue Cao(曹飞跃), Shuya Xing(邢淑雅), Haoyu Dong(董皓宇), Jianfeng Guo(郭剑锋), Shangzhi Gu(顾尚志), Yanyan Geng(耿燕燕), Shuo Mi(米烁), Hanxiang Wu(吴翰翔), Fei Pang(庞斐), Rui Xu(许瑞), Wei Ji(季威), and Zhihai Cheng(程志海)

Chin. Phys. B, 2021, 30 (**9**): 096804. DOI: 10.1088/1674-1056/ac11e8

Second-order topological insulator in twisted bilayer graphene with small twist angles

Fenghua Qi(戚凤华)[1], Jie Cao(曹杰)[2,†], Xingfei Zhou(周兴飞)[3,‡], and Guojun Jin(金国钧)[4,5,§]

[1] *School of Electronic Engineering, Nanjing Xiaozhuang University, Nanjing* 211171, *China*
[2] *College of Mechanics and Engineering Science, Hohai University, Nanjing* 210098, *China*
[3] *New Energy Technology Engineering Laboratory of Jiangsu Province School of Science, Nanjing University of Posts and Telecommunications, Nanjing* 210023, *China*
[4] *School of Physics Science and Technology, Kunming University, Kunming* 650214, *China*
[5] *National Laboratory of Solid State Microstructures, Department of Physics, and Collaborative Innovation Center of Advanced Microstructures, Nanjing University, Nanjing* 210093, *China*

(Received 24 May 2025; revised manuscript received 24 June 2025; accepted manuscript online 10 July 2025)

In recent years, the study of higher-order topological states and their material realizations has become a research frontier in topological condensed matter physics. We demonstrate that twisted bilayer graphene with small twist angles behaves as a second-order topological insulator possessing topological corner charges. Using a tight-binding model, we compute the topological band indices and corner states of finite-sized twisted bilayer graphene flakes. It is found that for any small twist angle, whether commensurate or incommensurate, the gaps both below and above the flat bands are associated with nontrivial topological indices. Our results not only extend the concept of second-order band topology to arbitrary small twist angles but also confirm the existence of corner states at acute-angle corners.

Keywords: second-order topological insulators, twisted bilayer graphene

PACS: 68.65.Cd, 73.20.At, 03.65.Vf

DOI: 10.1088/1674-1056/adee03 **CSTR:** 32038.14.CPB.adee03

1. Introduction

A recent experimental breakthrough is the fabrication of twisted bilayer graphene (TBG) with accurately controlled twist angles, followed by the discoveries of superconductivity and a strongly correlated Mott insulating state in such a system.[1–4] One notable feature in the band structure of TBG is the presence of nearly flat bands at a series of magic twist angles due to strong interlayer coupling.[5–17] The reduced kinetic energy of the flat bands enhances the effect of Coulomb interactions and drives the system into a strongly correlated phase.[18–32] According to the low-energy theory of TBG, where intervalley mixing is neglected, there are two Dirac points at each corner of the moiré Brillouin zone (MBZ), whose origin can be traced back to the Dirac points at the same valley of a graphene monolayer (GML). Because the two Dirac points from the same valley possess the same chirality, the flat bands carry nonzero Chern numbers, which introduces an obstruction to constructing an effective Wannier description of the flat bands.[33,34] Several works have proposed that this Wannier obstruction is fragile, meaning that it can be removed after one or more trivial bands are added to the effective model. This fragile topology in TBG can be interpreted as a higher-order topology when more bands are considered.[35,36]

The concept of a higher-order topological insulator requires that the band topology of a d-dimensional insulator manifests as nontrivial d–2 or lower-dimensional boundary states.[37–47] In the case of TBG, which is a two-dimensional system, higher-order topology implies the existence of corner modes in the system gaps. As recently shown by Park *et al.*,[48] TBG with large twist angles has been identified as a second-order topological insulator (SOTI),[48–54] where the system gap at charge neutrality originates from intervalley scattering. On the other hand, in the small twist-angle regime, which has drawn most of the research attention, the two inequivalent valleys are well separated from each other. The gaps at the Dirac points in pristine TBG can thus be safely neglected. However, near the first magic angle, the lowest flat bands are well separated from high-energy bands due to the corrugation effect. These gaps above and below the flat bands offer an opportunity to explore TBG at small twist angles as a candidate material for a two-dimensional SOTI.

In this paper, we investigate the corner modes around the densities $n = \pm 2n_s$ at small twist angles, corresponding to the full filling of the conduction (valence) flat bands. Here, n_s denotes the density of one electron per moiré unit cell, and spin freedom is not considered. Since the long-period moiré interference pattern at the first magic angle contains more than 11000 atoms per unit cell, it is a challenging problem to rig-

†Corresponding author. E-mail: caojie@hhu.edu.cn
‡Corresponding author. E-mail: zxf@njupt.edu.cn
§Corresponding author. E-mail: gjin@nju.edu.cn

© 2025 Chinese Physical Society and IOP Publishing Ltd. All rights, including for text and data mining, AI training, and similar technologies, are reserved.

orously solve the single-electron wave equation in real space. An alternative approach is to increase the twist angle while maintaining the topology of the flat bands. However, because the electronic band structure of TBG depends sensitively on the twist angle θ, an artificially enhanced corrugation must be introduced to preserve the isolation of the flat bands when θ is larger than the first magic angle. Using a real-space tight-binding model, we calculate the topological band indices and the gapped topological corner states in a finite-size TBG system. We find that these indices and corner states can identify small-twist-angle TBG as a SOTI. Although B. Liu *et al.* have already shown that the full-filling gaps are topologically nontrivial,[51] we extend this conclusion to any incommensurate angles and demonstrate that more than one type of corner state exists in these gaps. Specifically, our numerical results reveal that these gaps host both 120° and 60° corner states, in contrast to the single type of corner state typically observed in previous studies.[48,51] This diversity of corner states directly arises from the topological protection provided by the nontrivial second Stiefel–Whitney number, which remains robust even in incommensurate systems where the moiré pattern lacks translational symmetry. Moreover, we demonstrate that the second Stiefel–Whitney number of these gaps remains identical to that of the inter-flat-band gap,[48] owing to the preserved valley U(1) and C_{2z} symmetries. This finding highlights the pivotal role of lattice symmetries in stabilizing higher-order topological phases within TBG. These results significantly broaden the understanding of topological states in twisted systems and provide a new avenue for exploring exotic quantum phenomena in two-dimensional materials.

The paper is organized as follows. In Section 2, we describe small-twist-angle TBG using the real-space tight-binding model. In Section 3, we calculate the topological band indices and gapped topological corner states at commensurate angles. In Section 4, we study the gapped topological corner states at arbitrary twist angles. Finally, we present brief conclusions in Section 5.

2. Real space lattice model

We construct a TBG by rotating layer 1 and layer 2 by angles $-\theta/2$ and $+\theta/2$, respectively, in a fully overlapping graphene bilayer. The moiré unit cell is spanned by L_1 and L_2, as illustrated in Fig. 1(a). The lattice constant $|L_1| = |L_2| = L$ is given by $L = a/(2\sin(\theta/2))$. The local stacking configuration resembles the regular arrangements such as AA, AB, or BA. In momentum space, the two Dirac points of the rotated graphene layers are separated by $k_\theta = 2K_0\sin(\theta/2)$, where $K_0 = 4\pi/(3a)$ and a is the lattice constant of each GML. After the band reconstruction, $+K_1$ and $-K_2$ are folded onto one corner ($\overline{K}'$) of the MBZ of the TBG, while $-K_1$ and $+K_2$ are folded onto the other inequivalent corner ($\overline{K}$), as shown in Figs. 1(b) and 1(c).

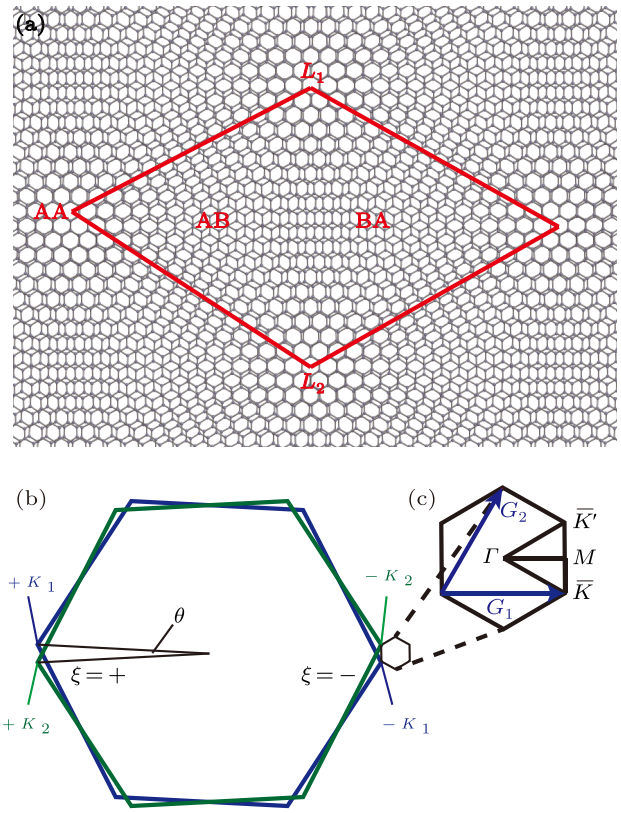


Fig. 1. Brillouin zone folding in TBG with a small twist angle θ. (a) Atomic structure of TBG at $\theta = 3.48°$. (b) The two large hexagons represent the first BZs of the two GMLs, distinguished by blue (layer 1) and green (layer 2), where $\pm K_{1,2}$ denote the valleys in the respective BZs. (c) The small hexagon represents the MBZ of TBG, with $\overline{K}$ and $\overline{K}'$ indicating the valleys in the MBZ.

We use the p_z orbital of carbon atoms in a single-orbital tight-binding model.[14] The Hamiltonian is written as

$$H = -\sum_{i,j} t(\boldsymbol{R}_i - \boldsymbol{R}_j)|\boldsymbol{R}_i\rangle\langle\boldsymbol{R}_j| + \text{h.c.}, \tag{1}$$

where $\boldsymbol{R}_i$ and $|\boldsymbol{R}_i\rangle$ represent the lattice position and the atomic state at site i, respectively. We assume that the transfer integral between any two orbitals is expressed in the Slater–Koster form as

$$-t(\boldsymbol{R}) = V_{pp\pi}\left[1 - \left(\frac{\boldsymbol{R}\cdot\boldsymbol{e}_z}{R}\right)^2\right] + V_{pp\sigma}\left(\frac{\boldsymbol{R}\cdot\boldsymbol{e}_z}{R}\right)^2,$$
$$V_{pp\pi} = V^0_{pp\pi}\,\mathrm{e}^{-(R-a)/r_0},\ \ V_{pp\sigma} = V^0_{pp\sigma}\,\mathrm{e}^{-(R-d_0)/r_0}. \tag{2}$$

Here, $\boldsymbol{e}_z$ is the unit vector perpendicular to the graphene plane, $a \approx 0.142$ nm is the lattice constant, and $d_0 \approx 0.335$ nm is the interlayer spacing. The parameter $V^0_{pp\pi}$ denotes the transfer integral between the nearest-neighbor atoms within a graphene layer, while $V^0_{pp\sigma}$ corresponds to that between vertically aligned atoms in adjacent layers. We take $V^0_{pp\pi} \approx -2.7$ eV and $V^0_{pp\sigma} \approx 0.48$ eV to fit the dispersion of GML. The decay length of the transfer integral is $r_0 \approx 0.045$ nm, so that the next-nearest intralayer coupling becomes $0.1V^0_{pp\pi}$.

Earlier studies assumed a perfectly flat TBG,[14–16] but more detailed theoretical research has revealed that the optimized lattice structure of TBG is actually corrugated in the out-of-plane direction. Recent first-principles calculations predict that the interlayer distance increases (decreases) in the AA (AB/BA) stacking regions, with maximum (minimum) distances of ~ 0.368 nm (0.328 nm) near the first magic angle.[55] Such corrugation arises directly from the interplay between van der Waals interactions and the twisting of the two graphene layers. It induces sizable gaps between the lowest bands and higher bands, consistent with experimental observations and numerical results from the continuum model.[33] The corrugation-induced variation in interlayer distance can be described as

$$d = d_0 + d_c \sum_{i=1}^{3} \cos(\boldsymbol{G}_i \cdot \boldsymbol{r}), \tag{3}$$

where $\boldsymbol{G}_1 = k_\theta(\sqrt{3},0)$, $\boldsymbol{G}_2 = k_\theta(\sqrt{3}/2,3/2)$, and $\boldsymbol{G}_3 = \boldsymbol{G}_1 - \boldsymbol{G}_2$ are the reciprocal lattice vectors of the MBZ, as shown in Fig. 1(c). For the first magic angle, $d_c \sim 0.01$ nm.

At commensurate angles, there are approximately $1/\sin^2(\theta/2)$ atoms in one moiré unit cell. This number increases rapidly in the small-angle limit due to the long-period moiré interference pattern. It is therefore challenging to rigorously solve the single-electron wave equations for small twist angles. One approach is to calculate the low-energy band structure near the Dirac points of the GMLs by linearizing the intralayer Hamiltonians and introducing a cutoff in the superlattice Fourier space.[5,10,56] However, this continuum model cannot treat boundary problems. Another approach is to scale certain coupling energies by a suitable factor to obtain a similar low-energy band structure at a larger twist angle, leading to a smaller moiré unit cell.[57–59] When focusing on topology rather than flat bands, it is sufficient to rescale d_c while keeping other parameters unchanged. Our numerical calculations confirm that the band structures remain qualitatively similar for twist angles not exceeding 5°. As shown in Fig. 2, the energy gaps above and below the lowest bands are preserved with artificially enlarged d_c, while the valley U(1) symmetry remains intact precisely as in the continuum model.

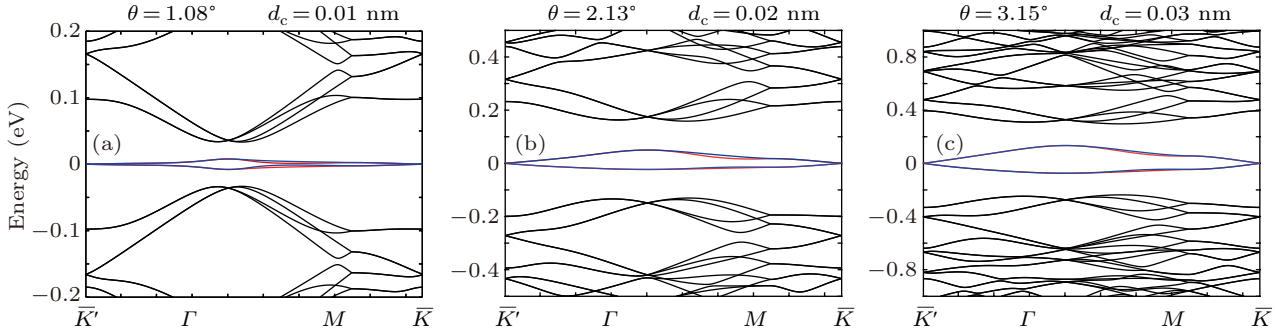


Fig. 2. Band structures of TBG at small twist angles. The lowest bands become nearly flat at the first magic angle $\theta = 1.08°$. As the twist angle increases, the lowest bands remain separated from the higher-energy bands by introducing an artificially enlarged interlayer corrugation d_c. Although this enlarged d_c deviates from the realistic configuration, it preserves the topological properties of the lowest bands at these twist angles.

3. Second-order topological insulator and corner states at commensurate angles

Using the tight-binding model at commensurate twist angles, we explore the SOTI phase by directly evaluating the second Stiefel–Whitney number. The TBG preserves the two-dimensional inversion symmetry C_{2z}, whose product with the time-reversal symmetry $\mathcal{T}$, i.e., $C_{2z}\mathcal{T}$, ensures that the Hamiltonian is characterized by the Stiefel–Whitney classes. While the Chern numbers associated with the energy gaps turn out to be trivial, the nontrivial second Stiefel–Whitney number ω_2 can be extracted from our tight-binding calculations. Following Ref. [48], ω_2 is defined in terms of the number of occupied bands with odd parity, $N_{\rm occ}^-$, at the time-reversal-invariant momenta (TRIM) $\Gamma_i \in \{\Gamma, M_1, M_2, M_3\}$ as

$$(-1)^{\omega_2} = \prod_{\Gamma_i} (-1)^{N_{\rm occ}^-(\Gamma_i)/2}. \tag{4}$$

At small twist angles, the valley U(1) symmetry effectively suppresses intervalley mixing. Within each valley, the Dirac points remain gapless and protected by the combined $C_{2z}\mathcal{T}$ symmetry, leading to metallic behavior at half filling. Meanwhile, the corrugation effect separates the lowest bands from the higher ones. The energy gaps above and below these lowest bands are associated with nontrivial second Stiefel–Whitney numbers. As shown in Figs. 3(a) and 3(b), we numerically confirm $\omega_2 = 1$ and observe the corresponding corner states for $\theta = 4.41°$ with an enlarged corrugation amplitude $d_c = 0.04$ nm.

The existence of SOTI phases associated with these energy gaps can, in fact, be generalized to all small commensurate angles. The argument proceeds in two steps.

Step one We summarize the result that the second Stiefel–Whitney number must be nontrivial at half filling for any commensurate angle.[48] In general, for commensurate angles, the area of the monolayer Brillouin zone (BZ) always contains $2N+1$ ($N \in \mathbb{Z}$) MBZs. For example, Fig. 3(c) illustrates that the monolayer BZ covers seven MBZs at $\theta = 21.78°$. Accord-

ingly, there exist $2N+1$ occupied states at each TRIM point $\boldsymbol{X}$ in the MBZ, corresponding to $2N+1$ "non-TRIM" points in the unfolded monolayer BZ. These points are related to the monolayer TRIM point $\boldsymbol{X}_{00}$ through

$$\boldsymbol{X}_{mn} = \boldsymbol{X}_{00} + m\boldsymbol{G}_1 + n\boldsymbol{G}_2, \tag{5}$$

where m,n are integers. At half filling, the states originating from these points are singly occupied. Note that $\boldsymbol{X}_{mn}$ and $\boldsymbol{X}_{-m,-n}$ are connected by inversion symmetry. If we choose the basis of the occupied states at the TRIM points in the MBZ as $(|\boldsymbol{X}_{00}\rangle, |\boldsymbol{X}_{01}\rangle, |\boldsymbol{X}_{0,-1}\rangle, \ldots, |\boldsymbol{X}_{mn}\rangle, |\boldsymbol{X}_{-m,-n}\rangle)$, the inversion operator $\hat{C}_{2z}$ in the MBZ can be expressed as

$$\hat{C}_{2z} = \begin{pmatrix} \zeta(\boldsymbol{X}_{00}) & 0 \\ 0 & \sigma_x \otimes I_N \end{pmatrix}, \tag{6}$$

where $\zeta(\boldsymbol{X}_{00})$ denotes the inversion eigenvalue of the occupied state at $\boldsymbol{X}_{00}$ in the GML. Clearly, the contributions from $\boldsymbol{X}_{m\neq0,n\neq0}$ cancel out, and the second Stiefel–Whitney number is determined by the inversion eigenvalues at the TRIM points inherited from the GML

$$(-1)^{\omega_2} = \zeta(\boldsymbol{M}_1)\zeta(\boldsymbol{M}_2)\zeta(\boldsymbol{M}_3)\zeta(\boldsymbol{\Gamma}). \tag{7}$$

In the GML, the inversion eigenvalues at the $\boldsymbol{M}$ and $\boldsymbol{\Gamma}$ points always differ by a sign, and therefore the second Stiefel–Whitney number is guaranteed to be nontrivial at half filling.

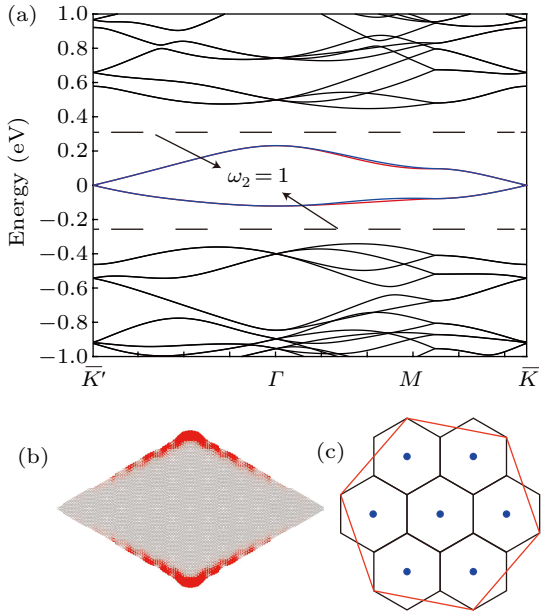


Fig. 3. TBG with $\theta = 4.41^\circ$ and $d_c = 0.04$ nm. (a) The energy gaps above and below the flat bands are topologically nontrivial, characterized by the second-order topological invariant $\omega_2 = 1$. (b) Corner state near the filling $n = 2n_s$ under mirror-symmetric open boundary conditions. The TBG flake consists of 8×8 moiré unit cells containing a total of 43264 atoms. The size of the red circles indicates the amplitude of the wave function, clearly showing that the corner state is localized at the obtuse corners. (c) Monolayer BZ and MBZ at $\theta = 21.78^\circ$. The blue dots denote the Γ_{mn} points, while other TRIM points are not shown.

Step two We prove that the gaps (if present) above and below the flat bands are also associated with nontrivial second Stiefel–Whitney numbers at small commensurate angles. In this case, it suffices to consider only the lowest conduction (valence) band in comparison with the half-filling scenario. Since the TRIM points from different valleys are related by inversion symmetry, i.e., $\hat{C}_{2z}|\Gamma_i\rangle_\xi = |\Gamma_i\rangle_{\bar{\xi}}$, one can construct a new basis composed of symmetric and antisymmetric superpositions of the degenerate states in the lowest bands

$$|\psi(\Gamma_i)\rangle_\pm = |\Gamma_i\rangle_\xi \pm |\Gamma_i\rangle_{\bar{\xi}}, \tag{8}$$

where ξ denotes the valley index. These basis states satisfy the relations $\hat{C}_{2z}|\psi(\Gamma_i)\rangle_\pm = \pm|\psi(\Gamma_i)\rangle_\pm$. At each TRIM point, there exists one state with odd parity in the lowest conduction (valence) bands. Consequently, the number of occupied bands with odd parity changes by four when the Fermi energy is shifted above (or below) the lowest bands, and thus the second Stiefel–Whitney number remains unchanged according to Eq. (4).

It is worth emphasizing that the SOTI phase is protected by crystalline symmetry rather than time-reversal symmetry, consistent with the conclusions of Ref. [48]. The Stiefel–Whitney number is determined by summing the number of wavefunctions with odd parity at all TRIM points for the occupied bands. For small twist angles, the system retains the valley U(1) symmetry. When the Fermi level moves from the energy gap between the two flat bands to either the gap above or below them, it crosses two entire flat bands. Due to the valley U(1) symmetry, there is no coupling between these two flat bands, and they are related to each other through the C_{2z} symmetry. Our analysis shows that at each TRIM point, these two wavefunctions combine into one even-parity and one odd-parity state. Since there are four TRIM points in the MBZ, the two flat bands collectively contribute four wavefunctions with odd parity at the TRIM points. Therefore, the energy gaps both above and below the flat bands, as well as the gap between them, share the same Stiefel–Whitney number, giving rise to topological corner states.

Once either the valley U(1) symmetry or the C_{2z} symmetry is broken, the above argument no longer holds. Nevertheless, this does not imply that the two central flat bands themselves are topologically trivial. On the contrary, previous studies on magic-angle TBG have demonstrated that, under the protection of valley U(1) and C_{2z} symmetries, the two flat bands originating from different valleys carry opposite Chern numbers, confirming that they are indeed topologically nontrivial.[12–14]

4. Generalization to an arbitrary twist angle

In general, the twist angle can be an arbitrary value rather than a commensurate one. If the twist angle becomes incommensurate, the TBG loses its translational symmetry, and the momentum can no longer be strictly defined. Consequently, the topological band theory breaks down in such a

case. However, any incommensurate angle can be approximated by a commensurate one within the experimental uncertainty $\delta\theta \sim 0.01^\circ$.

A commensurate moiré pattern can be characterized by two integers m and n, which are related to the twist angle θ as[5]

$$\cos\theta = \frac{3m^2+3mn+n^2/2}{3m^2+3mn+n^2}. \tag{9}$$

Accordingly, for an arbitrary twist angle, one can find a sufficiently close commensurate approximation by solving

$$\frac{m}{n} \sim -\frac{1}{2} + \sqrt{\frac{1+\cos\theta}{12(1-\cos\theta)}}. \tag{10}$$

For instance, an incommensurate angle $\theta = 4.53^\circ$ can be approximated by a commensurate angle $\theta = 4.529^\circ$ with $m = 34$ and $n = 5$. Substituting the incommensurate angle with its commensurate counterpart restores the translational symmetry and the applicability of topological band theory, so that the second Stiefel–Whitney number can be well defined.

On the other hand, as long as $n \neq 1$, one moiré unit cell contains multiple AA regions and the lattice constant L becomes significantly enlarged. Nevertheless, the distance between neighboring AA regions can still be approximated as $L_{\mathrm{AA}} = a/(2\sin(\theta/2))$, and so can the corrugation period. As shown in the continuum model, the low-energy band structure varies continuously with the twist angle, and so does the band topology.

5. Robustness of corner states in incommensurate and disordered systems

When the twist angle slightly deviates from a commensurate value, as long as the bulk gap remains open, the topology of the gap should remain unchanged. In Fig. 4, we numerically confirm the existence of corner states near the filling $n = 2n_{\mathrm{s}}$ for four incommensurate twist angles. Even though the sizes of the TBG flakes are much smaller than the moiré unit cells associated with the approximated commensurate angles, the flake length scales are still much larger than the corrugation period L_{AA}. Therefore, we can safely conclude that the second-order topology persists for arbitrarily small twist angles, provided that the valley U(1) symmetry remains unbroken.

In Fig. 5, we further present the energy spectra of finite-size TBG flakes and identify the corner states. We find a series of eigenstates appearing within the energy ranges corresponding to the bulk-state energy gaps (gray shaded regions). All of these states are localized at the flake boundaries, confirming the topological nature of the two energy gaps. In each gap, we observe four corner states. Interestingly, unlike most of the corner states reported in previous studies, which are predominantly 120° corner states, our calculations reveal both 120° and 60° corner states. In addition, near the Dirac points, two low-energy corner states are also found, consistent with the conclusion in Ref. [48].

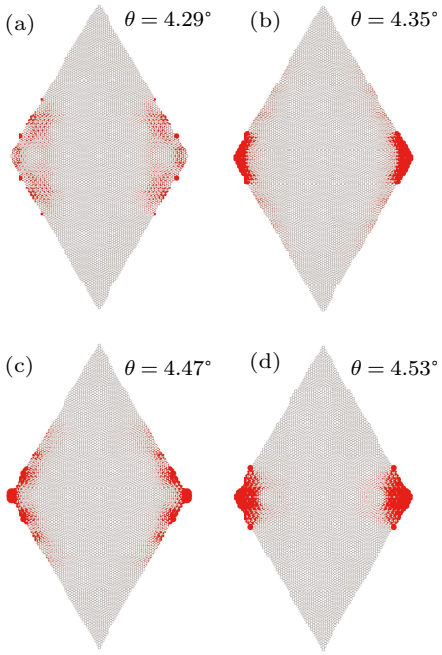


Fig. 4. Numerical results of the corner states under symmetric open boundary conditions for different incommensurate twist angles. The side length of each flake is approximately $6L_{\mathrm{AA}}$, with the rotation center fixed at the center of the flake. The corresponding approximated commensurate angles are: (a) $\theta = 4.294^\circ$ with $m = 36$ and $n = 5$, (b) $\theta = 4.344^\circ$ with $m = 64$ and $n = 9$, (c) $\theta = 4.475^\circ$ with $m = 62$ and $n = 9$, and (d) $\theta = 4.529^\circ$ with $m = 34$ and $n = 5$. The size of each circle represents the weight of the corresponding corner-state wave function.

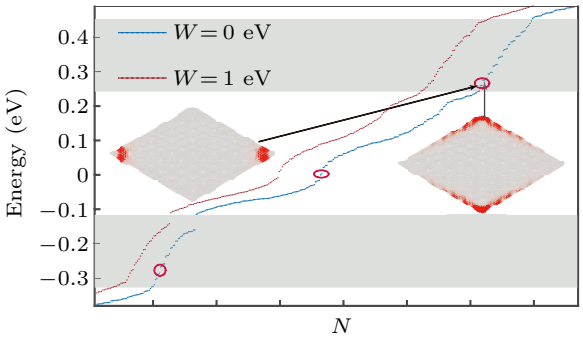


Fig. 5. Energy spectrum of a TBG flake with $\theta = 4.41^\circ$ and $d_{\mathrm{c}} = 0.04$ nm, under disorder strengths of $W = 0$ (blue) and $W = 1$ eV (red). The shaded regions indicate the bulk energy gaps, within which the eigenstates are localized along the edges or at the corners. Among these, the points circled in red denote the corner states.

To evaluate the robustness of the corner states in the presence of disorder, we introduce a random on-site potential modeled as $U_i = W\omega_i$, where ω_i is a uniformly distributed random variable in the interval $[-0.5, 0.5]$, and W controls the disorder strength. By applying exact diagonalization to the tight-binding model, we perform a comprehensive numerical analysis of how the corner states evolve under increasing disorder. Our results demonstrate a remarkable property: even when the disorder strength reaches $W = 1$ eV — a relatively high value for this system — the corner states remain within the band gaps, as shown in Fig. 5. The number of corner states in

each gap stays constant, underscoring their topological robustness. This observation agrees with the theoretical prediction that topologically protected states are immune to local perturbations.

However, the influence of disorder is not entirely negligible. While the existence of corner states persists, their degeneracy is gradually lifted as W increases. The initially degenerate corner states begin to split in energy, indicating an onset of delocalization, where their wave functions originally confined to specific corners start to spread spatially. This splitting signifies that although the topological protection of corner states remains intact, their spatial confinement weakens under strong disorder. These results offer valuable insights into the interplay between topology and disorder, revealing the fundamental mechanisms that govern the behavior of higher-order topological states in disordered systems.

6. Conclusion

In this work, we have performed a comprehensive numerical investigation of corner modes in TBG with small twist angles. At the carrier density $n = \pm 2n_s$, corresponding to the full filling of the conduction (valence) flat bands, we find four corner states residing within the associated energy gaps.

To rigorously solve the single-electron wave equation in real space, we propose an alternative approach for computing the topological band index. This is achieved by gradually increasing the twist angle while maintaining the flat bands separated from the other bands. Given that the electronic band structure of TBG is highly sensitive to the twist angle θ, we introduce an artificially enhanced corrugation when θ is larger than the first magic angle to preserve the isolation of the flat bands. Using a real-space tight-binding model, we calculate both the topological band index and the gapped topological corner states in finite-size TBG flakes.

Our results reveal that the topological band index and the gapped corner states consistently identify the small-angle TBG as a SOTI. Furthermore, we extend this conclusion to incommensurate twist angles and demonstrate that four corner states persist within the energy gaps — two corresponding to 120° corners and two to 60° corners. These findings highlight the robustness of higher-order topology in TBG against twist-angle incommensurability.

Acknowledgment

This work was supported by the National Natural Science Foundation of China (Grant Nos. 12104232 and 12074156).

References

[1] Cao Y, Fatemi V, Fang S, Watanabe K, Taniguchi T, Kaxiras E and Jarillo-Herrero P 2018 *Nature* **556** 43
[2] Cao Y, Fatemi V, Demir A, Fang S, Tomarken S L, Luo J Y, Sanchez-Yamagishi J D, Watanabe K, Taniguchi T, Kaxiras E, Ashoori R C and Jarillo-Herrero P 2018 *Nature* **556** 80
[3] Yankowitz M, Chen S, Polshyn H, Zhang Y, Watanabe K, Taniguchi T, Graf D, Young A F and Dean C R 2019 *Science* **363** 1059
[4] Lu X, Stepanov P, Yang W, Xie M, Aamir M A, Das I, Urgell C, Watanabe K, Taniguchi T, Zhang G, Bachtold A, MacDonald A H and Efetov D K 2019 *Nature* **574** 653
[5] Lopes dos Santos J M B, Peres N M R and Castro Neto A H 2007 *Phys. Rev. Lett.* **99** 256802
[6] Hass J, Varchon F, Millán Otoya J E, Sprinkle M, Sharma N, de Heer W A, Berger C, First P N, Magaud L and Conrad E H 2008 *Phys. Rev. Lett.* **100** 125504
[7] Li G, Luican A, Lopes dos Santos J M B, Castro Neto A H, Reina A, Kong J and Andrei E Y 2010 *Nat. Phys.* **6** 109
[8] Miller D L, Kubista K D, Rutter G M, Ruan M, de Heer W A, First P N and Stroscio J A 2010 *Phys. Rev. B* **81** 125427
[9] Luican A, Li G, Reina A, Kong J, Nair R R, Novoselov K S, Geim A K and Andrei E Y 2011 *Phys. Rev. Lett.* **106** 126802
[10] Bistritzer R and MacDonald A H 2011 *Proc. Natl. Acad. Sci. USA* **108** 12233
[11] Lopes dos Santos J M B, Peres N M R and Castro Neto A H 2012 *Phys. Rev. B* **86** 155449
[12] Moon P and Koshino M 2012 *Phys. Rev. B* **85** 195458
[13] Trambly de Laissardi'ere G, Mayou D and Magaud L 2012 *Phys. Rev. B* **86** 125413
[14] Moon P and Koshino M 2013 *Phys. Rev. B* **87** 205404
[15] Koshino M 2015 *New J. Phys.* **17** 015014
[16] Koshino M and Moon P 2015 *J. Phys. Soc. Jpn.* **84** 121001
[17] Xu Y and Jin G 2015 *Europhys. Lett.* **111** 67006
[18] Xu C and Balents L 2018 *Phys. Rev. Lett.* **121** 087001
[19] Rademaker L and Mellado P 2018 *Phys. Rev. B* **98** 235158
[20] Dodaro J F, Kivelson S A, Schattner Y, Sun X Q and Wang C 2018 *Phys. Rev. B* **98** 075154
[21] Wu F, Lovorn T, Tutuc E and MacDonald A H 2018 *Phys. Rev. Lett.* **121** 026402
[22] Po H C, Zou L, Vishwanath A and Senthil T 2018 *Phys. Rev. X* **8** 031089
[23] Pizarro J M, Calderón M J and Bascones E 2019 *J. Phys. Commun.* **3** 035024
[24] Isobe H, Yuan N F Q and Fu L 2018 *Phys. Rev. X* **8** 041041
[25] Liu C C, Zhang L D, Chen W Q and Yang F 2018 *Phys. Rev. Lett.* **121** 217001
[26] Kennes D M, Lischner J and Karrasch C 2018 *Phys. Rev. B* **98** 241407
[27] Guo H, Zhu X, Feng S and Scalettar R T 2018 *Phys. Rev. B* **97** 235453
[28] You Y Z, Vishwanath A 2019 *npj Quantum Mater.* **4** 16
[29] Irkhin V Y and Skryabin Y N 2018 *JETP Lett.* **107** 651
[30] Zhang Y H, Mao D, Cao Y, Jarillo-Herrero P and Senthil T 2019 *Phys. Rev. B* **99** 075127
[31] Wu F and Das Sarma S 2020 *Phys. Rev. Lett.* **124** 046403
[32] Zhang Y H, Mao D and Senthil T 2019 *Phys. Rev. Res.* **1** 033126
[33] Koshino M, Yuan N F Q, Koretsune T, Ochi M, Kuroki K and Fu L 2018 *Phys. Rev. X* **8** 031087
[34] Kang J and Vafek O 2018 *Phys. Rev. X* **8** 031088
[35] Po H C, Watanabe H and Vishwanath A 2018 *Phys. Rev. Lett.* **121** 126402
[36] Po H C, Zou L, Senthil T and Vishwanath A 2019 *Phys. Rev. B* **99** 195455
[37] Benalcazar W A, Bernevig B A and Hughes T L 2017 *Phys. Rev. B* **96** 245115
[38] Langbehn J, Peng Y, Trifunovic L, von Oppen F and Brouwer P W 2017 *Phys. Rev. Lett.* **119** 246401
[39] Song Z, Fang Z and Fang C 2017 *Phys. Rev. Lett.* **119** 246402
[40] Parameswaran S A and Wan Y 2017 *Physics* **10** 132
[41] Lin Z K, Wu S Q, Wang H X and Jiang J H 2020 *Chin. Phys. Lett.* **37** 074302
[42] Zhang Y, Su Z, Wang Y and Huang L 2023 *Appl. Phys. Lett.* **123** 221102
[43] Li J, Deng C, Zhang K, Lu Q and Yang H 2023 *Appl. Phys. Lett.* **123** 253101
[44] Yang Y, Chen X, Pu Z, Wu J, Huang X, Deng W, Lu J and Liu Z 2024 *Phys. Rev. B* **109** 165406
[45] Han Y, Cui C, Li X P, Zhang T T, Zhang Z, Yu Z M and Yao Y 2024 *Phys. Rev. Lett.* **133** 176602
[46] Tu W, Wu Y J, Liu C C and Li N 2023 *EPL* **142** 16002

[47] Zhang C and Mei J 2023 *Europhys. Lett.* **142** 26003
[48] Park M J, Kim Y, Cho G Y and Lee S 2019 *Phys. Rev. Lett.* **123** 216803
[49] Ahn J, Park S and Yang B J 2019 *Phys. Rev. X* **9** 021013
[50] Liu B B, Zeng X T, Chen C, Chen Z and Sheng X L 2022 *Phys. Rev. B* **106** 035153
[51] Liu B, Xian L, Mu H, Zhao G, Liu Z, Rubio A and Wang Z F 2021 *Phys. Rev. Lett.* **126** 066401
[52] Hua C B, Xiao F, Liu Z R, Sun J H, Gao J H, Chen C Z, Tong Q, Zhou B and Xu D H 2023 *Phys. Rev. B* **107** L020404
[53] Wan X, Zeng J, Zhu R, Xu D H, Zheng B and Wang R 2025 *Phys. Rev. B* **111** 085137
[54] Hua C and Xu D H 2025 *Chin. Phys. B* **34** 037301
[55] Lucignano P, Alfè D, Cataudella V, Ninno D and Cantele G 2019 *Phys. Rev. B* **99** 195419
[56] Tarnopolsky G, Kruchkov A J and Vishwanath A 2019 *Phys. Rev. Lett.* **122** 106405
[57] Su Y and Lin S Z 2018 *Phys. Rev. B* **98** 195101
[58] Gonzalez Arraga L A, Lado J L, Guinea F and San Jose P 2017 *Phys. Rev. Lett.* **119** 107201
[59] Julku A, Peltonen T J, Liang L, Heikkilä T T and Törmä P 2020 *Phys. Rev. B* **101** 060505